Acta Crystallographica Section D
Biological Crystallography
ISSN 0907-4449

Neutron and X-ray structural studies of short hydrogen bonds in photoactive yellow protein (PYP)

S. Z. Fisher,[a]* S. Anderson,[b] R. Henning,[c] K. Moffat,[c] P. Langan,[a] P. Thiyagarajan[d] and A. J. Schultz[d]

[a]Bioscience Division, Los Alamos National Laboratory, M888, Los Alamos, NM 87545, USA, [b]Molecular Pharmacology and Biological Chemistry, Northwestern University Feinberg School of Medicine, Chicago, IL 60611, USA, [c]Department of Biochemistry and Molecular Biology, Institute for Biophysical Dynamics and the Center for Advanced Radiation Sources, The University of Chicago, 929 East 57th Street, Chicago, IL 60637, USA, and [d]Intense Pulsed Neutron Source, Argonne National Laboratory, Argonne, IL 60439, USA

Correspondence e-mail: zfisher@lanl.gov

Received 10 August 2007
Accepted 27 September 2007

PDB Reference: photoactive yellow protein, 2qws, r2qwssf.

Photoactive yellow protein (PYP) from *Halorhodospira halophila* is a soluble 14 kDa blue-light photoreceptor. It absorbs light *via* its *para*-coumaric acid chromophore (pCA), which is covalently attached to Cys69 and is believed to be involved in the negative phototactic response of the organism to blue light. The complete structure (including H atoms) of PYP has been determined in D_2O-soaked crystals through the application of joint X-ray (1.1 Å) and neutron (2.5 Å) structure refinement in combination with cross-validated maximum-likelihood simulated annealing. The resulting XN structure reveals that the phenolate O atom of pCA accepts deuterons from Glu46 $O^{\varepsilon 2}$ and Tyr42 O^{η} in two unusually short hydrogen bonds. This arrangement is stabilized by the donation of a deuteron from Thr50 $O^{\gamma 1}$ to Tyr42 O^{η}. However, the deuteron position between pCA and Tyr42 is only partially occupied. Thus, this atom may also interact with Thr50, possibly being disordered or fluctuating between the two bonds.

1. Introduction

Photoactive yellow protein (PYP) from *Halorhodospira halophila* is a cytosolic 14 kDa blue-light photoreceptor (125 amino acids) that belongs to the PAS-domain superfamily (Taylor & Zhulin, 1999). Blue light is absorbed by a *para*-coumaric acid chromophore, pCA, which is covalently attached to Cys69. The absorption spectrum of PYP is similar to the wavelength-dependent negative phototactic behavior of *H. halophila*, thus implicating PYP in this biological response (Sprenger *et al.*, 1993). After PYP absorbs a photon in the ground state (P), it converts quickly to a red-shifted intermediate (I_1). It subsequently converts to a bleached blue-shifted species (I_2) and eventually returns to P to complete the photocycle (Meyer *et al.*, 1993). During the reversible photocycle, activated PYP transduces photon energy into a structural change that involves *trans*-to-*cis* isomerization of the pCA chromophore and ultimately causes rearrangement of the active-site hydrogen-bond pattern and the tertiary structure of the protein, in particular its N-terminal helices. We believe that these structural changes may also be relevant to the photocycles of other systems (Genick *et al.*, 1997; Rajagopal *et al.*, 2005; Ihee *et al.*, 2005).

In the ground state, the chromophore in the *trans* conformation is stabilized by two hydrogen bonds involving its

© 2007 International Union of Crystallography
Printed in Denmark – all rights reserved

phenolate O atom with Tyr42 O^{η} (∼2.7 Å) and Glu46 O^{ε} (∼2.7 Å) (Borgstahl *et al.*, 1995). Subsequent structural analyses at higher resolution (Anderson *et al.*, 2004) concluded that these hydrogen bonds were quite unusually short, at 2.49 ± 0.01 Å and 2.58 ± 0.01 Å, respectively. Tyr42 and Glu46 have unusual pK_a values, such that at pH ≃ 7.0 the phenolate oxygen of pCA is deprotonated and Tyr42 and Glu46 are protonated, most likely as a consequence of desolvation and hydrogen-bonding effects (Kim *et al.*, 1995; Xie *et al.*, 1996). Hydrogen bonding in the chromophore-binding pocket is thought to be crucial to photocycle kinetics (Anderson *et al.*, 2004). An understanding of the exact nature of this hydrogen bonding would be greatly enhanced by determining the detailed distribution of H atoms in the binding site. High-resolution X-ray crystal structures of PYP provide accurate distances for possible hydrogen bonds, but no definitive information on the positions of H atoms (Anderson *et al.*, 2004). Neutron diffraction can provide this information because, unlike X-rays, neutrons are readily scattered by H atoms.

The possible implication of short strong hydrogen bonds (SSHB) in PYP has been discussed previously by Anderson *et al.* (2004). As hydrogen bonds become shorter, the barrier between the two protonation sites is expected to decrease. The resulting low-barrier hydrogen bonds (LBHB) have been proposed to be important in some enzymatic reaction mechanisms (Cleland, 2000). A characteristic of SSHBs is lengthening of the donor O—H covalent bond (Steiner & Saenger, 1994) and possible disorder over two protonation sites with the decrease in the barrier, eventually leading to a centered single-well potential for very short hydrogen bonds.

Using neutron crystallography, it has already been possible to locate H atoms in the active site of several proteins, providing unique information on their structure and mechanism and the factors underlying enhanced substrate binding (Schoenborn, 1969; Norvell *et al.*, 1975; Kossiakoff & Spencer, 1980; Phillips & Schoenborn, 1981; Wlodawer *et al.*, 1983; Coates *et al.*, 2003; Niimura *et al.*, 1997; Katz *et al.*, 2006; Bennett *et al.*, 2006). Neutron crystallography has also provided detailed information on the hydration of proteins, including the exact coordination of water molecules (Kossiakoff, 1985; Blakeley *et al.*, 2004; Kurihara *et al.*, 2004). Furthermore, neutron crystallography can be used to identify which H atoms can be readily replaced by deuterium (D) and the extent of this replacement, thus providing a tool for the study of protein dynamics that is complementary to NMR techniques. Nevertheless, the practical application of neutrons to protein crystallography has been limited in the past by the relatively weak flux of beamlines, in particular compared with synchrotron X-ray beamlines, the requirement for large crystals (>1 mm^3) and a lack of dedicated beamlines for protein crystallography at high-flux neutron sources.

Here, we present the results of a neutron protein crystallography study of PYP. In this study, we have successfully collected time-of-flight (*i.e.* wavelength-resolved) Laue neutron data to 2.5 Å from a small (0.79 mm^3) crystal equilibrated against D_2O-containing mother liquor using the PCS beamline at Los Alamos Neutron Science Center (LANSCE) pulsed spallation source (Langan *et al.*, 2004). As H atoms account for nearly half of the atoms in a protein, adding H atoms in a neutron structure refinement increases the number of parameters and reduces the data-to-parameter ratio, thus increasing the danger of overfitting and decreasing the accuracy of the optimized model. This problem is particularly acute in the current study because of the medium resolution of the diffraction data. We have therefore used the approach, originally developed for macromolecular crystallography by Wlodawer & Hendrickson (1982), of combining the neutron data with 1.1 Å X-ray data in a joint (XN) structure refinement.

Another advantage of joint XN structure refinement is that displaying both X-ray and neutron scattering density maps together greatly aids their interpretation. In particular, hydrogenated C atoms do not appear in 2.5 Å neutron scattering density maps because of cancellation by the negative neutron scattering of H atoms, but do appear in X-ray scattering density maps. Water molecules are also easier to orient using information on the O-atom position from the X-ray scattering density map and information on the complete D_2O molecule from the neutron scattering density map.

On the basis of the XN structure, we discuss the hydrogen bonding in the binding site, its implication for the photocycle of PYP and the dynamics of PYP as derived from H/D-exchange patterns in the protein.

Table 1
Neutron data collection from PCS at LANSCE: data set and refinement statistics.

Values in parentheses are for the highest resolution shell. The statistics of the 1.1 Å X-ray data set are as reported by Anderson *et al.* (2004) and the original X-ray structure was deposited as PDB entry 1otb.

Crystal settings	15
Space group	$P6_3$
Unit-cell parameters (Å)	a = 66.83, c = 40.95
Resolution (Å)	30.0–2.5 (2.64–2.50)
Total No. of reflections	10615 (1103)
Unique reflections	3172 (410)
Redundancy	3.3 (2.7)
Completeness (%)	88.8 (79.3)
$\langle I/\sigma(I)\rangle$	3.4 (1.7)
R_{sym}†	0.312 (0.413)
Unique reflections for $I/\sigma(I) > 5$	2458 (245)
Completeness (%) for $I/\sigma(I) > 5$	68.4 (47.3)
R_{sym}† for $I/\sigma(I) > 5$	0.238 (0.285)
No. of protein atoms	1105
No. of solvent atoms	77
R.m.s.d. bond lengths (Å)	0.005
R.m.s.d. bond angles (°)	0.922
Average B factors (Å^2)	
Main chain	15.5
Side chain	17.9
Solvent	30.0
pCA	12.8
R_{cryst}‡/R_{free}§	
X-ray only	0.214/0.230
Neutron only	0.262/0.273
Joint XN	0.216/0.232

† $R_{sym} = \sum|I - \langle I\rangle|/\sum\langle I\rangle$. ‡ $R_{work} = \sum|F_o - F_c|/\sum|F_o|$. § R_{free} is calculated in the same way as R_{work} for data omitted from refinement (5% of reflections for all data sets).

2. Materials and methods

2.1. Sample preparation and crystallization

Wild-type PYP from *H. halophila* (strain BN9626) was heterologously expressed as a His-tagged apoprotein as described previously (Kort *et al.*, 1996; Anderson *et al.*, 2004). The overexpressed protein was affinity-purified using nickel chromatography. Subsequent to purification, the His tag was removed by incubation with TEV protease at room temperature. The protein purity was evaluated by SDS–PAGE. Prior to crystallization, the sample was concentrated to 30 mg ml^{-1}. Crystals of wild-type PYP were prepared in space group $P6_3$ using a microseeding technique and 2.6 *M* ammonium sulfate in 50 m*M* sodium phosphate pH 7.0 (McRee *et al.*, 1989).

2.2. Data collection and processing

Room-temperature neutron data of PYP in the dark state were collected from a large (1.8 × 0.7 × 0.63 mm; 0.79 mm^3) single crystal of wild-type PYP mounted in a quartz capillary. The labile H atoms were exchanged with D atoms by incubating the crystal for over a month in 3.2 *M* deuterated ammonium sulfate in D_2O; the deuterated stabilization buffer was replaced weekly to maximize the amount of exchange. Time-of-flight wavelength-resolved Laue diffraction images were collected at PCS at LANSCE over 15 crystal settings with 22 h exposure times per setting. The sample-to-detector distance was 70 cm and all images were collected at room temperature. Data were processed with a version of *d*TREK* modified for wavelength-resolved Laue diffraction images (Pflugrath, 1999; Langan & Greene, 2004). The wavelength distribution range used for data processing was 0.9–4.5 Å. The data were wavelength-normalized with the program *LAUENORM* (Helliwell *et al.*, 1989) using only reflections with $I > 6\sigma$ to determine the wavelength-normalization scaling curve. The data were merged to 2.5 Å resolution using the program *SCALA* from the *CCP*4 suite of programs (Weiss, 2001; Collaborative Computational Project, Number 4, 1994), with an overall completeness of 89%. Although the merging statistics are high (R_{sym} = 31%), this is offset to some extent by a data redundancy of greater than 3. The lower value of 23.8% for R_{sym} calculated using only neutron intensities with $I/\sigma(I) > 5$

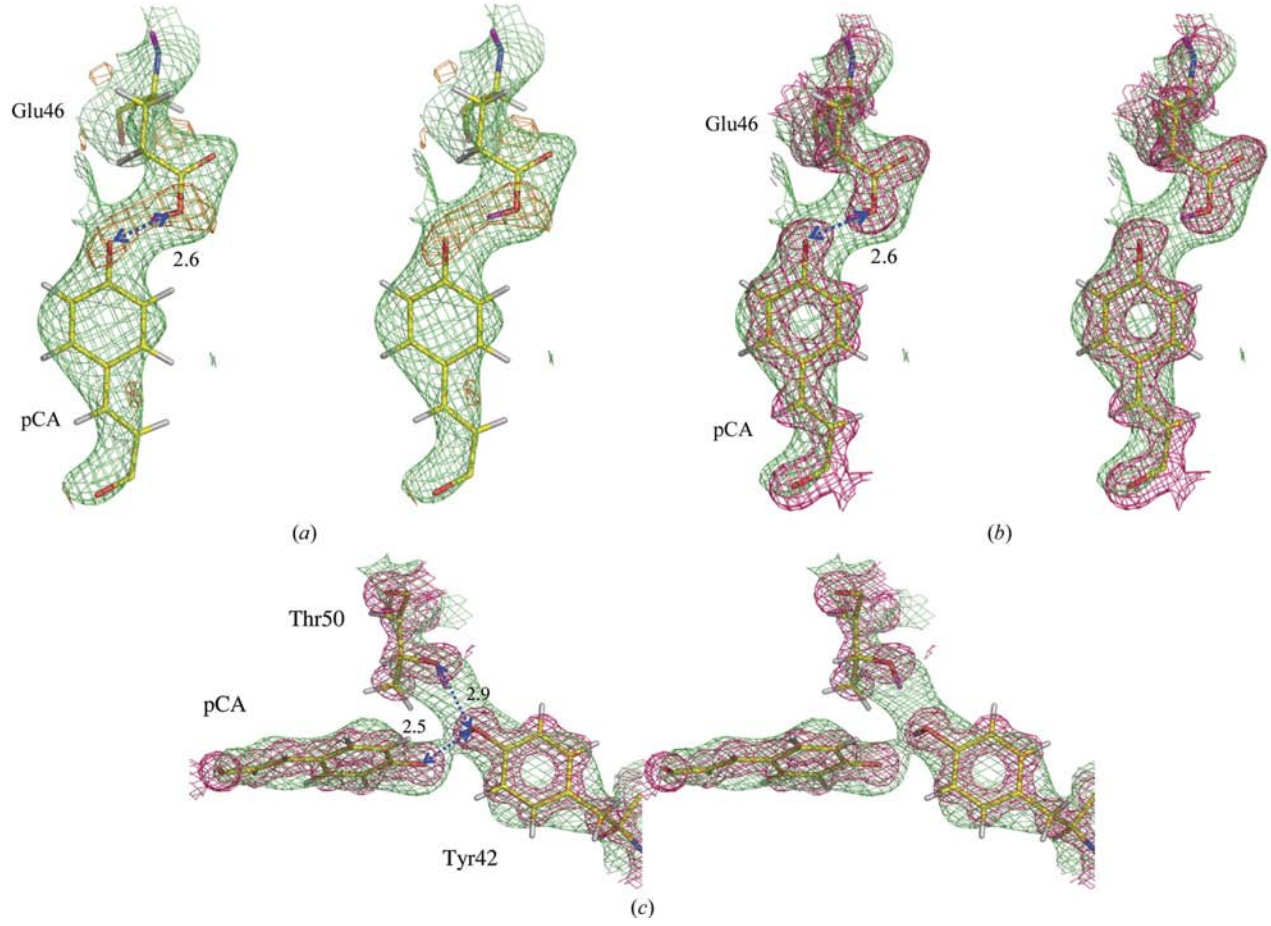

Figure 1
Cross-eye stereoview of the chromophore-binding pocket and active-site architecture. (*a*) Hydrogen bond between Glu46 and pCA; (*b*) hydrogen bond between Glu46 and pCA; (*c*) hydrogen bond between pCA, Thr50 and Tyr42. Binding-pocket residues and pCA are shown in yellow ball-and-stick representation. The $2F_o - F_c$ nuclear map is shown in green mesh (contoured at 1.2σ), the $F_o - F_c$ nuclear map in orange and the $2F_o - F_c$ electron-density map in red mesh (contoured at 1.2σ). Blue arrows indicate hydrogen bonds.

indicates that there are no worrying systematic errors in the data. Data-set and data-collection statistics are given in Table 1.

2.3. Structure refinement

The structure was refined using a version of *CNS* (Brünger *et al.*, 1998) called *nCNS* modified for joint X-ray and neutron refinement (M. Mustyakimov *et al.*, manuscript in preparation). In *nCNS*, XN structure refinement is combined with recent developments in the use of cross-validated maximum-likelihood simulated-annealing refinement. The starting model used for refinement was a wild-type room-temperature structure of PYP (PDB code 1otb; Anderson *et al.*, 2004). Following simulated annealing, a combination of positional, individual temperature-factor and grouped and individual occupancy refinement was used. *nCNS* was then used to refine water positions and occupancies and also the occupancies of the backbone amide H atoms. To assess the degree of exchange of the backbone amides, H atoms (neutron scattering length $b_{\rm H} = -3.739$ fm) were manually replaced with D atoms ($b_{\rm D} = 6.671$ fm) in the PDB file and the occupancies were refined between −0.56 (unexchanged, hydrogen) and 1.00 (fully exchanged, deuterium), −0.56 being the relative scattering length of H compared with D. The occupancy of each water molecule was refined as a group. Modeling of water orientations was aided by examining potential hydrogen-bond donors and acceptors. The final model contained 1105 non-H/D atoms, 1080 H/D atoms and 68 water molecules, all modeled as D_2O. The statistics of the refinement are reported in Table 1.

3. Results and discussion

3.1. The chromophore-binding pocket

The phenolate O atom of pCA accepts hydrogen bonds from protonated Glu46 $O^{\varepsilon2}$ and Tyr42 O^{η} (Fig. 1). This arrangement is stabilized by Thr50 $O^{\gamma1}$ donating a hydrogen bond to Tyr42 O^{η} and accepting a hydrogen bond from Arg52 N^{α}. The H atom of Thr50 N^{α} has not been exchanged with D, whereas the N^{α} H atoms of the two neighboring residues, Ile49 and Gly51, are fully exchanged by D. The N^{α} H atoms of Ile49, Thr50 and Gly51 are hydrogen bonded to the O^{α} atoms of Ala45, Glu46 and Gly47, respectively. The fact that Thr50 N^{α} does not undergo H/D exchange suggests that it is involved in a particularly stable hydrogen bond with Glu46.

The D atom of Tyr42 O^{η} does not refine to an ideal position for hydrogen bonding to pCA, but rather points slightly away from the phenolate O atom (Fig. 1*c*). Whereas there is strong nuclear density indicating the presence of D atoms between Thr50 $O^{\gamma1}$ and Tyr42 O^{η} and between Glu46 $O^{\varepsilon2}$ and pCA, the nuclear density between Tyr42 O^{η} and pCA is much weaker (Fig. 1). As a negative control, a D atom covalently attached to the phenolate oxygen of pCA was included and, as expected, its occupancy refined to zero, confirming that pCA is not protonated. Two Fourier difference maps, calculated first with the corresponding D atoms omitted and then with the corresponding O atoms omitted, display positive nuclear density only between Thr50 $O^{\gamma1}$ and Tyr42 O^{η} and between Glu46 $O^{\varepsilon2}$ and pCA. These maps suggest that the D atom between Tyr42 O^{η} and pCA only partially occupies that position. To investigate this further, we refined the occupancy of the corresponding D atoms in two possible hydrogen-bonding configurations: Glu46 $O^{\varepsilon2}$-D1···pCA, Tyr42 O^{η}-D2···pCA

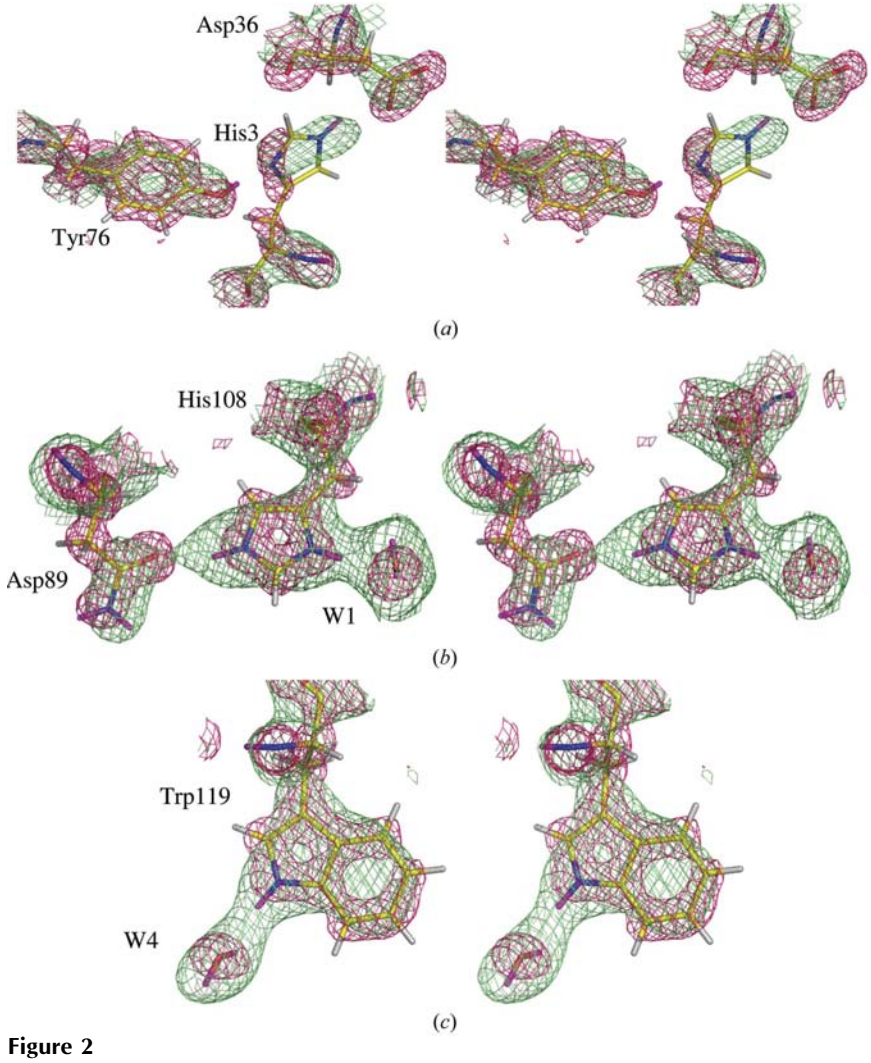

Figure 2
Cross-eye stereoview of solvent and protonated-residue interactions. (*a*) Interaction between His3, Asp36 and Tyr76; (*b*) interaction of protonated His108 and Asp89 with W1; (*c*) interaction of protonated Trp119 with W4. The $2F_{\rm o} - F_{\rm c}$ electron-density maps are shown in red mesh (contoured at 1.5σ) and the $2F_{\rm o} - F_{\rm c}$ nuclear density in green mesh (contoured at 1.5σ).

and Thr50 Oγ1-D3$\cdots$Tyr42 O$^{\eta}$ (designated configuration 1) and Glu46 Oε2-D1$\cdots$pCA, Tyr42 O$^{\eta}$-D2$\cdots$Thr50 O$^{\gamma1}$ and Thr50 O$^{\gamma1}$-D3$\cdots$Tyr42 O$^{\eta}$ (designated configuration 2). The occupancies of D1, D2 and D3 refined to 0.6, 0.6 and 1.0, respectively, for configuration 1, and 0.7, 1.0 and 1.0, respectively, for configuration 2. These results suggest that at room temperature and under the pH and solvent conditions of crystallization used in this study, the D atom on Tyr42 O$^{\eta}$ is either mobile or disordered between hydrogen bonds to pCA and Thr50. However, this is unexpected for such a short strong hydrogen bond. Another possibility to consider is that the H atom on Tyr42 did not fully exchange and is complicating the interpretation of the Fourier maps. The only practical way around this would be to determine the neutron structure of PYP under fully deuterated conditions with no H-atom contamination.

3.2. Protonation states

In addition to the protonation state of Glu46 in the binding site, the XN structure reveals the protonation states of other residues. In Fig. 2(*a*), His3 N$^{\varepsilon2}$ is protonated and donates a hydrogen bond to Asp36 O$^{\delta1}$. His3 N$^{\delta1}$ is deprotonated and accepts a hydrogen bond from Tyr76 O$^{\eta}$ of a neighboring molecule. The protonation state of His3 would therefore appear to be directly determined by this crystal-packing interaction. On the other hand, as shown in Fig. 2(*b*), His108 is doubly protonated and donates hydrogen bonds to Asn89 O$^{\delta1}$ and to the O of water W1. Trp119, the only tryptophan residue in PYP, is protonated and donates a hydrogen bond to the O of W4 (Fig. 2*c*). This information is not directly available from the high-resolution X-ray structure alone.

3.3. Side-chain localization

It is often difficult in X-ray crystallography to accurately orient the side chains of Asn and Gln residues, as the X-ray scattering powers of N and O atoms are very similar. However, as can be seen in Fig. 3(*a*), the N$^{\delta2}$ atom of Asn13 scatters neutrons much more strongly than X-rays (compare the red and blue densities) and makes determination of the orientation of these residues much easier and more accurate. Another interesting structural feature can be observed for Lys side chains. The nuclear density shown in Fig. 3(*b*) clearly shows that Lys110 is fully protonated. However, the hydrogenated (*i.e.* non-exchanged) C atoms of this side chain do not appear in the neutron map because of cancellation of the positive scattering from C (b_C = 6.646 fm) by the negative scattering of H atoms. The electron-density map for this side chain is clearly visible, illustrating the complementary nature of neutron and X-ray data for a particular structure.

3.4. Backbone H/D exchange of amide groups

Through occupancy refinement of D atoms found on backbone amides, it is possible to map the level of exchange onto the structure. Figs. 4(*a*) and 4(*b*) show a topology and ribbon representation to indicate the level of exchange. For the topology diagram three levels of exchange are indicated (D occupancies of 0.01–0.29 in light gray, 0.30–0.59 in dark gray and 0.60–1.00 in black; Pro residues are in blue), while for the ribbon diagram a continuous color gradient is used (blue, completely non-exchanged; red, completely exchanged). The β-sheet motif of the core domain of the protein undergoes the least amount of H/D exchange, with only 33% of the residues being fully exchanged. This is also the part of the structure that has the lowest thermal mobility, as reflected in the X-ray *B* factors. The helices that decorate the surface of PYP undergo a much higher extent of H/D exchange, with 65% of the residues being fully exchanged. These helices are largely in contact with solvent in the crystal, which most likely contributes to the higher extent of exchange. This is in agreement with previous neutron studies of proteins, which show the β-sheet motif to be relatively resistant to H/D exchange compared with the α-helix motif (Bennett *et al.*, 2006).

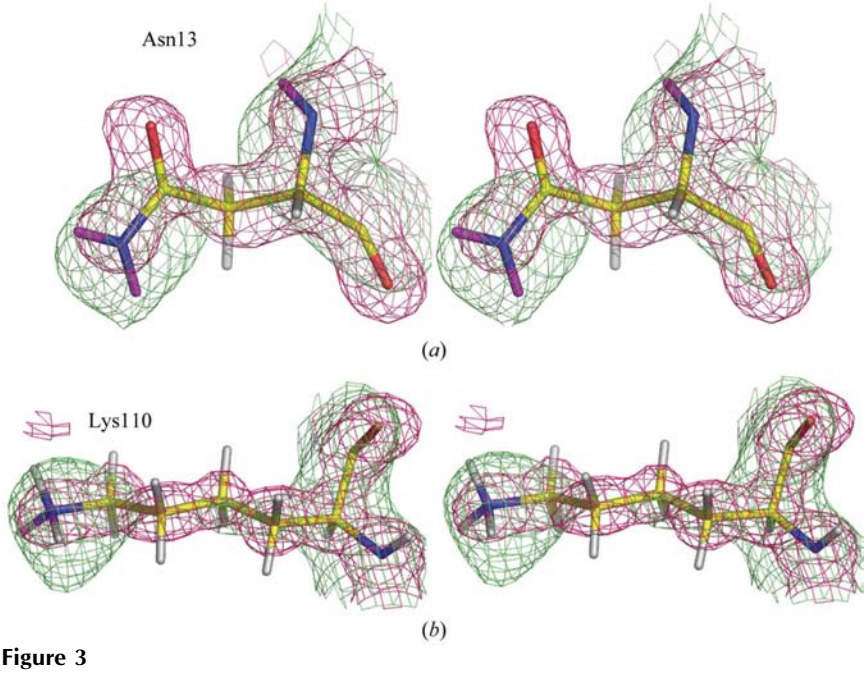

Figure 3
Cross-eye stereoview of side-chain localization. (*a*) Asn13 placement in nuclear density; (*b*) Lys110 is fully protonated and D density is clearly seen in neutron maps. The $2F_o - F_c$ electron-density maps are shown in red mesh (contoured at 1.2σ) and the $2F_o - F_c$ nuclear density in green mesh (contoured at 1.2σ).

4. Conclusion

PYP is a vital protein that serves as a useful and general model for characterizing and understanding light-dependent signal transduction and a simple photocycle. Investi-

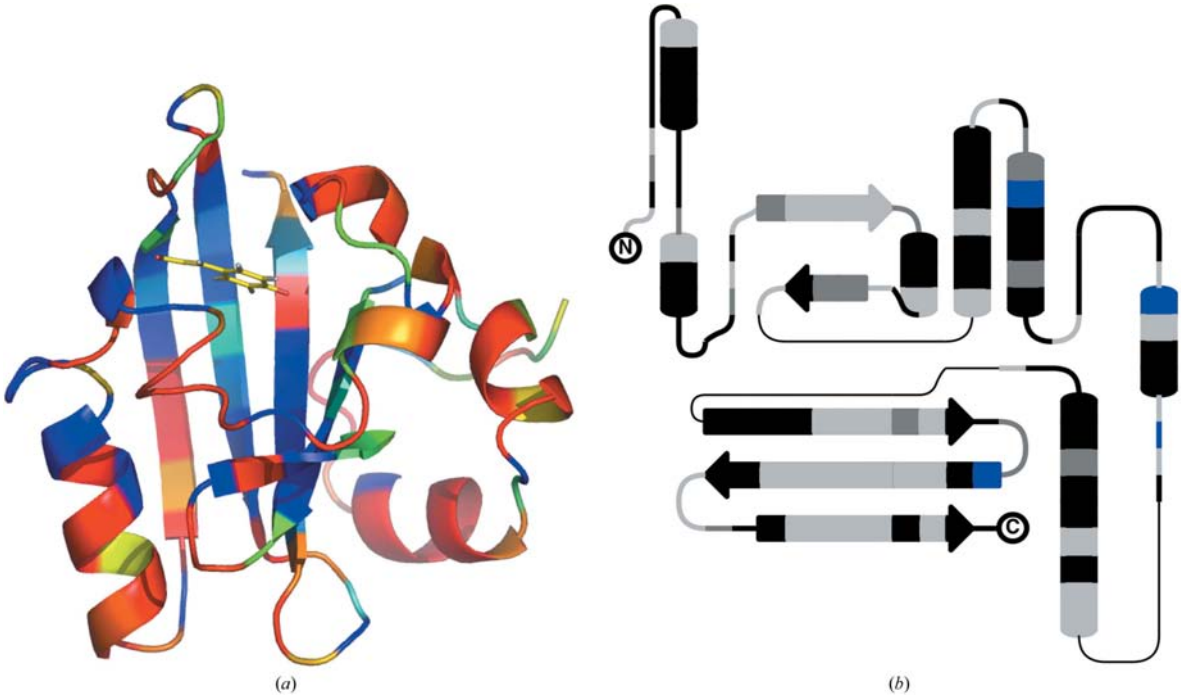

Figure 4
Extent of amide H/D exchange of PYP. (*a*) A topology representation of PYP indicating the extent of H/D exchange at backbone amide groups. Color scheme to show D occupancy: light gray, 0.01–0.29; dark gray, 0.30–0.59; black, 0.60–1.00; blue, Pro residues. (*b*) Ribbon diagram of PYP indicating exchange as in (*a*). Color scheme: blue, non-exchanged; red, fully exchanged. This figure was generated using *TopDraw* and *PyMOL* (Bond, 2003; DeLano, 2002).

gating key hydrogen bonds in the chromophore-binding pocket using neutron diffraction methods yields significant new information. The size of the crystal reported here is relatively small for a neutron study and this, in combination with the relatively weak flux of the neutron beam compared with X-rays, most likely contributed to limiting the diffraction to only 2.5 Å resolution (Blum *et al.*, 2007).

The results from this study are consistent with previous data in that pCA is involved in a strong hydrogen bond with Glu46. However, at room temperature and the pH of crystallization in this study, it appears that Tyr42 O^{η} does not bond exclusively with pCA, but that the corresponding deuteron may fluctuate between interactions with pCA and Thr50. This observation could also be a consequence of this H atom not fully exchanging. This is the first time direct evidence for these interactions have been observed. The crystals used here diffracted neutrons to only 2.5 Å resolution, but even this modest resolution permits accurate structure refinement by combining the neutron data with X-ray data using the refinement software *nCNS*. The resulting structure is sufficiently accurate to observe solvent–protein and hydrogen-bonding interactions. This is in contrast to the atomic resolution (∼1 Å) structure obtained using X-rays, in which crucial details of the chromophore–protein interactions were still elusive (Anderson *et al.*, 2004). However, at 2.5 Å resolution with neutron protein crystallography on its own it is not possible to identify the short hydrogen bond as an LBHB, although the results are consistent with this possibility. Overall, the combination of joint X-ray and neutron protein crystallography has proven to be most fruitful for elucidating these hydrogenation details in PYP.

The PCS is funded by the Office of Science and the Office of Biological and Environmental Research of the US Department of Energy. MM and PL were partly supported by MNC (Macromolecular Neutron Crystallography), an NIH-NIGMS-funded consortium (1R01GM071939-01) between Los Alamos National Laboratory and Lawrence Berkeley National Laboratory to develop computational tools for neutron protein crystallography. KM and SA were supported by NIH grant GM036452. Work at Argonne National Laboratory was supported by the US Department of Energy, Office of Science, Office of Basic Energy Sciences under contract DE-AC02-06CH11357.

References

Anderson, S., Crosson, S. & Moffat, K. (2004). *Acta Cryst.* D**60**, 1008–1016.
Bennett, B., Langan, P., Coates, L., Mustyakimov, M., Schoenborn, B. P., Howell, E. & Dealwis, C. (2006). *Proc. Natl Acad. Sci. USA*, **103**, 18493–18498.
Blakeley, M. P., Kalb, A. J., Helliwell, J. R. & Myles, D. A. (2004). *Proc. Natl Acad. Sci. USA*, **101**, 16405–16410.
Blum, M.-M., Koglin, A., Rüterjans, H., Schoenborn, B., Langan, P. & Chen, J. C.-H. (2007). *Acta Cryst.* F**63**, 42–45.
Bond, C. S. (2003). *Bioinformatics*, **19**, 311–312.
Borgstahl, G. E., Williams, D. R. & Getzoff, E. D. (1995). *Biochemistry*, **34**, 6278–6287.

Brünger, A. T., Adams, P. D., Clore, G. M., DeLano, W. L., Gros, P., Grosse-Kunstleve, R. W., Jiang, J.-S., Kuszewski, J., Nilges, M., Pannu, N. S., Read, R. J., Rice, L. M., Simonson, T. & Warren, G. L. (1998). *Acta Cryst.* D**54**, 905–921.
Cleland, W. W. (2000). *Arch. Biochem. Biophys.* **382**, 1–5.
Coates, L., Erskine, P. T., Mall, S., Williams, P. A., Gill, R. S., Wood, S. P. & Cooper, J. B. (2003). *Acta Cryst.* D**59**, 978–981.
Collaborative Computational Project, Number 4 (1994). *Acta Cryst.* D**50**, 760–763.
DeLano, W. L. (2002). *PyMOL.* DeLano Scientific, Palo Alto, CA, USA.
Genick, U. K., Borgstahl, G. E. O., Ng, K., Ren, Z., Pradervand, C., Burke, P. M., Srajer, V., Teng, T.-Y., Schildkamp, W., McRee, D. E., Moffat, K. & Getzoff, E. D. (1997). *Science*, **275**, 1471–1475.
Helliwell, J. R., Habash, J., Cruickshank, D. W. J., Harding, M. M., Greenhough, T. J., Campbell, J. W., Clifton, I. J., Elder, M., Machin, P. A., Papiz, M. Z. & Zurek, S. (1989). *J. Appl. Cryst.* **22**, 483–497.
Ihee, H., Rajagopal, S., Srajer, V., Pahl, R., Anderson, S., Schmidt, M., Schotte, F., Anfinrud, P. A., Wulff, M. & Moffat, K. (2005). *Proc. Natl Acad. Sci. USA*, **102**, 7145–7150.
Katz, A. K., Li, X., Carrell, H. L., Hanson, B. L., Langan, P., Coates, L., Schoenborn, B. P., Glusker, J. P. & Bunick, G. J. (2006). *Proc. Natl Acad. Sci. USA*, **103**, 8342–8347.
Kim, M., Mathies, R. A., Hoff, W. D. & Hellingwerf, K. J. (1995). *Biochemistry*, **34**, 12669–12672.
Kort, R., Hoff, W. D., van West, M., Kroon, A. R., Hoffer, S. M., Vlieg, K. H., Crielaard, W. & Hellingwerf, K. J. (1996). *EMBO J.* **15**, 3209–3218.
Kossiakoff, A. A. (1985). *Annu. Rev. Biochem.* **54**, 1195–1227.
Kossiakoff, A. A. & Spencer, S. A. (1980). *Nature (London)*, **288**, 414–416.
Kurihara, K., Tanaka, I., Chatake, T., Adams, M. W., Jenney, F. E., Moiseeva, N., Bau, R. & Niimura, N. (2004). *Proc. Natl Acad. Sci. USA*, **101**, 11215–11220.
Langan, P. & Greene, G. (2004). *J. Appl. Cryst.* **37**, 253–257.
Langan, P., Greene, G. & Schoenborn, B. P. (2004). *J. Appl. Cryst.* **37**, 24–31.
McRee, D. E., Tainer, J. A., Meyer, T. E., van Beeumen, J., Cusanovich, M. A. & Getzoff, E. D. (1989). *Proc. Natl Acad. Sci. USA*, **86**, 6533–6537.
Meyer, T. E., Cusanovich, M. A. & Tollin, G. (1993). *Arch. Biochem. Biophys.* **306**, 515–517.
Niimura, N., Minezaki, Y., Nonaka, T., Castagna, J. C., Cipriani, F., Hoghoj, P., Lehmann, M. S. & Wilkinson, C. (1997). *Nature Struct. Biol.* **4**, 909–914.
Norvell, J. C., Nunes, A. C. & Schoenborn, B. P. (1975). *Science*, **190**, 568–570.
Pflugrath, J. W. (1999). *Acta Cryst.* D**55**, 1718–1725.
Phillips, S. E. V. & Schoenborn, B. P. (1981). *Nature (London)*, **292**, 81–82.
Rajagopal, S., Anderson, S., Srajer, V., Schmidt, M., Pahl, R. & Moffat, K. (2005). *Structure*, **13**, 55–63.
Schoenborn, B. P. (1969). *Nature (London)*, **224**, 143–146.
Sprenger, W. W., Hoff, W. D., Armitage, J. P. & Hellingwerf, K. J. (1993). *J. Bacteriol.* **175**, 3096–3104.
Steiner, T. & Saenger, W. (1994). *Acta Cryst.* B**50**, 348–357.
Taylor, B. L. & Zhulin, I. B. (1999). *Microbiol. Mol. Biol. Rev.* **63**, 479–506.
Weiss, M. S. (2001). *J. Appl. Cryst.* **34**, 130–135.
Wlodawer, A. & Hendrickson, W. A. (1982). *Acta Cryst.* A**38**, 239–247.
Wlodawer, A., Miller, M. & Sjölin, L. (1983). *Proc. Natl Acad. Sci. USA*, **80**, 3628–3631.
Xie, A., Hoff, W. D., Kroon, A. R. & Hellingwerf, K. J. (1996). *Biochemistry*, **35**, 14671–14678.